Nanoscale

Accepted Manuscript

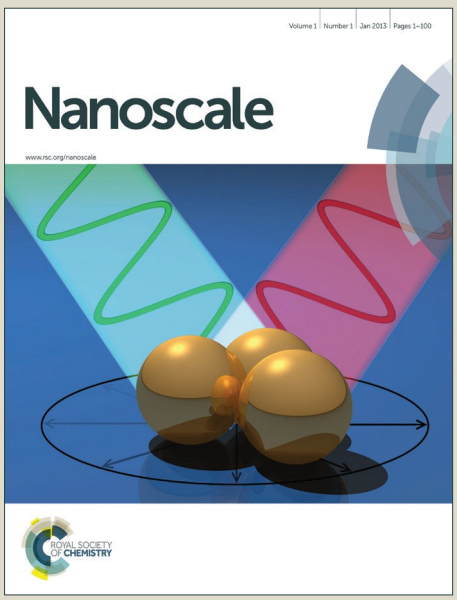

ROYAL SOCIETY OF CHEMISTRY

www.rsc.org/nanoscale

Journal Name

ARTICLE

Synthesis, characterization and enhanced gas sensing performance of porous $ZnCo_2O_4$ nano/microspheres

Received 00th January 20xx,
Accepted 00th January 20xx

DOI: 10.1039/x0xx00000x

www.rsc.org/

Tie Liu, [a] Jingyuan Liu,*[a] Qi Liu,[a] Dalei Song,[a] Hongseng Zhang, [a] Hongquan Zhang,[a,c] and Jun Wang*[a,b]

In recent years, spinel-type compounds have attracted great interest because of their gem-like qualities. However, little is known of their gas sensing properties. We report, in this paper, on a self-assembly method to prepare porous $ZnCo_2O_4$ (ZCO) nano/microspheres by a facile one-step solvothermal process and subsequent annealing. Abuntdant techniques were used to characterize the morphology and structure of the as-obtained compounds. Our data indicates that the hierarchical nano/microspheres are constructed from numerous nanoparticles primarily, which have higher specific surface area (ca. 77.3 $m^2 \cdot g^{-1}$) and are of uniform diameter (ca. 1μm). To demonstrate its potential application, the gas sensor based on as-synthesized ZCO nano/microspheres was fabricated to test its sensing performance, whose sensing behaviours correspond to p-typed semiconductors. The test results also indicate that porous spinel-type compounds have an exellent kinetic response to ethanol at an operating temperature of 175°C and a superior selectivity. As such, hierarchical porous $ZnCo_2O_4$ nano/microspheres will hold promising potential in the gas sensor field.

1. Introduction

Functional materials[1] with specific 3-D structures and advantageous physical and chemical properties, have great potential in every sphere of life, such as in the application of gas sensors[2], energy storage and transformation[3], catalysis[4], and in the field of medicinal chemistry[1]. Gas sensitive materials (GSMs) have attracted intense interest in sensors, whose sensing detection limit can achieve ppm, and even ppb level, which is more sensitive than animals, and euphemistically called "electronic nose".[5-7] Much effort has been directed into the design and control for the manufacture of GSMs with porous nano/microsphere structures,[8] which have beneficial properties such as higher specific area and favourable surface permeability for mass transportation.[8-15] For instance, porous SnO_2 was obtained and exhibited a high activity for detecting to volatile organic compounds (VOCs).[11] And there are also reports about TiO_2 nanomaterials for sensor applications.[12] However, those traditional GSMs, such as SnO_2[11, 12], TiO_2[12, 13], ZnO[13], α-Fe_2O_3[14], NiO[15], Co_3O_4[16], etc., still hardly meet people's demands for living requirements in some aspects, like higher operating temperature, longer response and recovery times, and poorer selectivity, restrict their applicability.[17-20] In recent years, to overcome these deficiencies, various multi-metal oxides have been tested and used in gas sensors, including $ZnFe_2O_4$, $NiFe_2O_4$, which are ternary compounds with a AB_2O_4 spinel structure.[21, 22] So, it is still extremely meaningful for further study those AB_2O_4-typed compounds to help resolve these issues and seek breakthrough.

Commonly, cobalt oxide (Co_3O_4), serving as an important functional material and possessing spinel-structure, has attracted considerable attention because it exhibits excellent gas sensitive properties, as reported in recent research studies.[20, 23-29] Even so, the gas sensitive material based on pure Co_3O_4 cannot fulfil the actual requirement, due to either a low selectivity or slow response speed, both restricting its application.[16, 30] Therefore, many techniques have been adopted to improve the gas sensing performance. Currently, more advanced technology involves either doping with precious components (such as Ag, Au, Pt, or Pb) or employing binary or ternary metal oxide semiconductors. Because of cobalt's toxicity and cost, recent efforts to modify cobalt oxide (Co_3O_4) have included partially replacing Co with more eco-friendly and cheaper alternative metal elements to form MCo_2O_4 (M = Cu, Zn, Ni, Mg, and Fe) without sacrificing its gas sensitive properties.[21, 31] Besides, two kinds of cobalt ions of variable valence exist which are suitable to obtain these compounds by replacement with equivalent metal ions without losing structural benefits. And for a hot functional gas sensing material (GSM), for example, zinc oxide (ZnO), a n-type semiconductor having higher exaction binding energy (60 meV) and wider band gap (3.2 eV), has been verified as a sensitive material to detect various gases, including C_2H_5OH, CH_3COCH_3, H_2, O_2, CO, H_2S, NO_2, NH_3, and other species.[13]

[a] Key Laboratory of Superlight Material and Surface Technology, Ministry of Education, Harbin Engineering University, 150001, PR China. E-mail: zhqw1888@sohu.com; Fax: +86 451 8253 3026; Tel: +86 451 8253 3026.
[b] Institute of Advanced Marine Materials, Harbin Engineering University, 150001, PR China.
[c] School of Automation, Harbin Engineering University, 150001, PR China.
†Electronic Supplementary Information (ESI) available. See DOI: 10.1039/x0xx00000x

Based on the above findings, we adopted another method to improve the gas sensing properties of Co_3O_4-based sensors. This was achieved by replacing Co^{2+} with Zn^{2+} to produce ZCO-typed sensor. A number of reports testify to the successful synthesis of a variety of similar compounds with spinel microstructure, like $NiCo_2O_4$, $ZnFe_2O_4$.[31-35] But to the best of our knowledge there are few reports about the synthesis and application of ZCO as GSMs. Therefore, the aim of the present study is to employ an appropriate method for the preparation of ZCO GSM with 3-D hierarchical structure. Wet chemical procedures combining subsequent thermal treatment have been successfully applied to prepare porous nano/microspheres. And crucially, hydrothermal techniques offer important favourable conditions, such as a low-cost, a simple synthetic route, excellent compositional control, high homogeneity at the molecular level, and mild crystallization temperature.[36, 42]

Herein, porous ZCO microspheres were obtained by an eco-friendly, template-free and one-step process. The porous (mesoporous[1] and macroporous) structures exhibited a large surface area, and favourable surface permeability for mass transportation, which effectively improved the gas sensing properties. We carried out a series of studies to make meaningful comparisons between the as-prepared samples. The test results ensured that ZCO showed a comparable advantage of gas sensing performance over Co_3O_4. So, ZCO has been identified as a more economical and environmental friendly replacement for Co_3O_4 as a novel GSM. The details were discussed as bellow.

2. Experimental section

2.1 Materials synthesis

All chemical reagents stated below were of analytical grade and used directly without any purification. The porous ZCO hollow compounds were obtained by a surfactant-free solvothermal process. Typically, we utilized Zn $(NO_3)_2 \cdot 6H_2O$ and Co $(NO_3)_2 \cdot 6H_2O$ as the metal sources. A moderate amount of Zn-Co mixture, with a mole ratio of 1:2, and 0.1g Na_2SO_4 powder was dispersed in 60 mL ethanol (Et)-ethylene glycol (Eg) mixed solution (volume ratio 2:5, forming L1) by an ultrasonic process for about 30s. A standard solution (0.67M) of urea was prepared using the same Et-Eg liquid system (forming L2). L2 was added to L1 dropwise, about a drop per 30s, to form a clear wine red solution (called L3), under vigorous magnetic stirring. Homogeneous L3 was transferred into a 100 ml Teflon-lined stainless-steel autoclave with 75% degree of filling and sealed. The autoclave was heated to 200°C and maintained at that temperature for 8 h, and then cooled to room temperature. The resulting ZnCo-precurser precipitates were systematically centrifuged and washed several times with deionized water and ethanol alternatively to remove possible superfluous cations and ions, and then dried in a vacuum at 70°C for 8 h. Following this, we employed a two-step calcined process in air with a heating rate of 2°C·min^{-1}, maintaining 400°C and 650°C for 2 h, respectively. Finally, an ultrafine powder (the target pure ZCO) was obtained after cooling down naturally, which was collected for characterization and further analysis. The Co_3O_4 microspheres were obtained by a similar process to the above but without the zinc sources added. The process to synthesize cubic ZCO was displayed in *Electronic Supporting Information*. Synthesis of ZCO nanoparticles was obtained by the similar process like reports before.[43, 44]

2.2 Characterization of materials

The as-obtained samples were characterized by X-ray diffraction (XRD, Rigaku TTR-III) with high-intensity Cu-Kα radiation (λ=0.15406 nm) operated at 40 kV and 150 mA to examine the crystal structure. The morphology and microstructure of samples were investigated by scanning electron microscopy (SEM, JEOL JSM-6480A) operated at an accelerating voltage of 20 kV. TEM and HRTEM images were carried out using a transmission electron microscope (FEITEM, Tecnai G220S-Twin) with accelerating voltages of 120 and 200 kV, respectively, to explore the internal structure further. Energy-dispersive X-ray spectrometry (EDS) was employed to research the chemical composition of the samples. The special surface structure of the ZCO porous nano/microsphere was evaluated by Brunauer–Emmett–Teller (BET) equation from a micrometrics ASAP 2010 M instrument at liquid nitrogen temperature. Pore size distribution was estimated using Barrett–Joyner–Halenda (BJH) method from the desorption isotherm. Thermo gravimetric (TG) analysis was carried out using a NETZSCH STA 409 PG/PC simultaneous thermo gravimetric analyser under air from 30 to 800°C with a heating rate of 10°C·min^{-1}. Surface chemical analysis of samples was performed by X-ray photoelectron spectroscopy (XPS, Thermo ESCALAB 250Xi). The products were degassed under vacuum at 150°C for 3 h before the gas sensing tests.

2.3 Fabrication and measurement of gas sensors

We prepared four gas sensors based on different kinds of sensing materials: ZCO porous nano/microspheres (denoted as "S1"), ZCO with cubic morphology (S2), pure Co_3O_4 peach like microspheres (S3), and ZCO nanoparticles (S4) to highlight the superiorities of ZCO porous nano/microspheres in gas sensing process. The preparation process of the gas sensor, taking S1 as an example, is described as follows (similar a little to that described in previous paper).[14] The as-prepared product S1 was dispersed into a specified amount of ethanol in an agate mortar with continued grinding to form homogeneous slurry and then coated onto an alumina tube, of diameter 1 mm and length 4 mm, where an electrode was connected with two Pt wires on each end. The thickness of coating was approximately 10μm. Next, a Ni-Cr alloy coil was inserted into the tube as a heater to control working temperature by tuning the heating voltage (V_h). The gas sensors, before the first measurement, were dried and aged for one day in air to improve their stability. Measurements of gas response were tested on a commercial NMDOG Multifunctional Precision Sensor Analysis Tester (Changsha Dingcheng Scientific Instrument Co., Ltd., Hunan, China), as detailed in the following.

To make the process clearer and easier to understand, the schematic diagrams, photograph and test circuit are shown in Fig. 1(a-c). The specific measurement was conducted by a

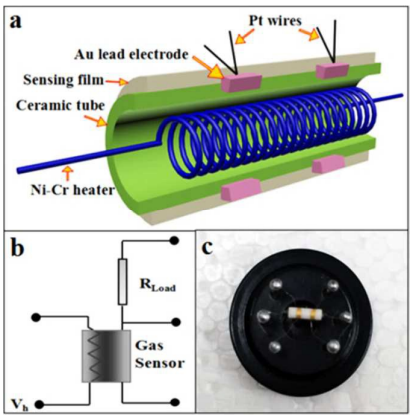

Fig. 1 Schematic diagram (a), the test circuit (b) and photograph image (c) of the gas sensor

static process: first, the sensor was put into a chamber filled with fresh air. Then a given amount of the test gas was injected into a closed chamber by a micro-syringe. Next the sensor was placed into the chamber for the measurement of sensing performance. When the response reached a constant value, the sensor was transferred into another chamber also filled with fresh air; it began to recover. With this measuring system, the steady-state value of conductivity was reached, and the response of the sensor measured again. For the calculation, the gas sensitivity (response) is defined as the ratio of Ga/Gg, where Ga and Gg are the conductivities measured in air and test gas atmosphere, respectively. The response and recovery times are defined as the time that the conductivity of gas sensor changes to 90% of the entire conductivity during target gas adsorption and desorption, respectively.

3. Results and discussion

3.1 Structural and morphological characteristics

The morphologies of the as-prepared products were investigated by SEM (Fig. 2a-f). As displayed, Fig. 2a and 2b show the panoramic pictures of S1, from which we can observe the well-dispersed ZCO microspheres with a relatively uniform diameter of about 0.5~1μm and some broken balls. Fig. 2c shows the rough, loose and porous surface feature of S1 (the enlarged image of labelled zone in Fig.2b); the larger surface area as well as numerous pores with a diameter of ~20 nm facilitate mass transport for gas diffusion. Besides, there are some broken spheres observed in Fig.2a and the enlarged single ZCO microsphere is displayed in Fig.2d, which show the hollow inner structure. Importantly, these porous and hollow balls can own two available surfaces (the inner and outer) in sensing process. The morphologies of compared samples (S2, S3) in Fig. 2e and Fig. 2f, display the microspheres (of peach-like appearance) and cubic features, respectively. And the SEM image of S4 was displayed in Fig.s4a, from which we can observe the nanoparticles with the size of 100nm and disordered morphology. To highlight the superior morphology and structure of S1 further, the low/high magnified TEM

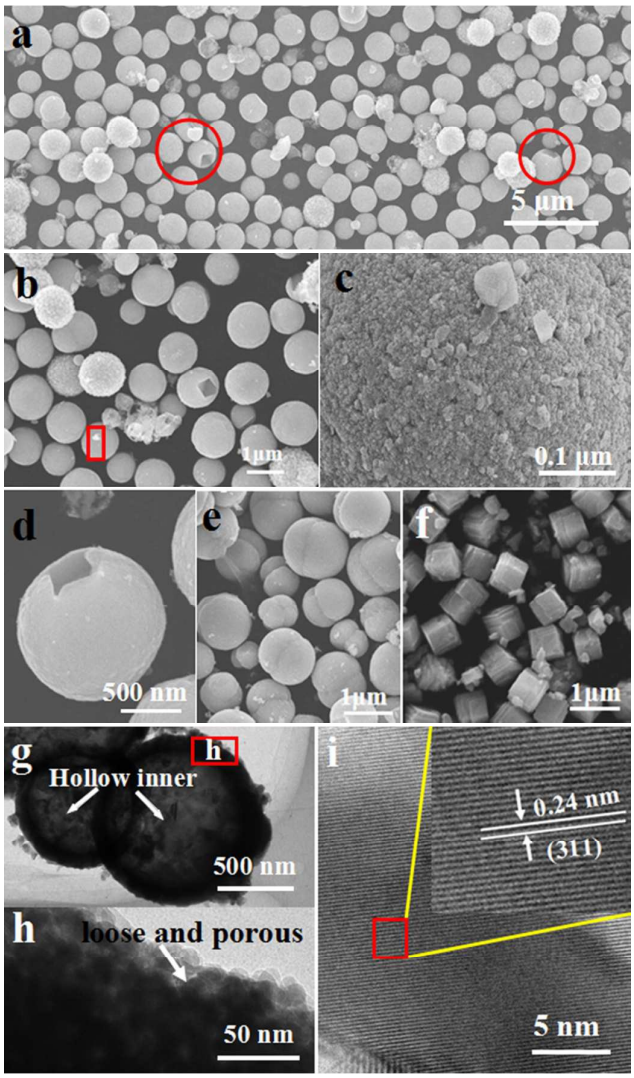

Fig. 2 Typical SEM images of three samples: ZCO microspheres (a), the enlarged image (b), the regional enlarged image of b (c), single broken ZCO microsphere (d), Co_3O_4 microspheres (e), laminar ZCO cubes (f), TEM of image of ZCO microspheres (g), the enlarged image of the red in g, (h), and HR-TEM image of corresponding area in h, (i).

images are shown in Fig. 2g~i, respectively. The typical TEM images (Fig. 2g and 2h) also exhibit a direct morphology of the as-obtained S1 to confirm the porous, loose and rough surfaces (highlighted by arrow) and hollow inner coupled with the SEM image (Fig. 2c and 2d, respectively), from which we also can observe microspheres with diameter of ~850nm. Subsequently, the corresponding HR-TEM images are displayed in Fig. 3i. The lattice fringes (inset) are clearly visible with a spacing distance of about 0.246nm between adjacent lattice planes, which matches well with the (311) plane of $ZnCo_2O_4$.[37]

The TG technique was performed to characterize the thermal properties and further determine the sintering temperature for the Zn-Co precursor. As shown in Fig. s2c, the total weight loss is about 34%. Three steps about the loss of mass in the TG curve: first, the loss of 4.3% at low temperature (below 100°C), which is attributed to the removal of physically absorbed water

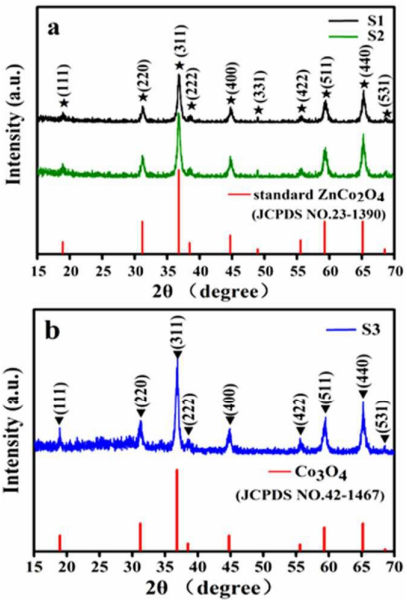

Fig. 3 XRD patterns of three samples: (a) S1 and S2, (b) S3.

in the temperature range of 30 to 90°C. In the next step, a drastic decrease, about 30% between 100 and 400°C, indicates a decomposition of the precursor. Finally, up to 500°C, the loss is less severe, showing the complete desorption of precursor.[32] Based on the analyses above, we chose 650°C as the final calcining heat for the preparation of $ZnCo_2O_4$ samples.[32, 38] Next, we present the XRD pattern of the porous ZCO microspheres in Fig. 3a. All the diffraction peaks of the ZCO sample match well with the standard card of cubic spinel ZCO (JCPDS No. 23-1390); no other diffraction peaks of additional impurities are present and lower figure of merit (FOM) both confirm its high purity. The sharp and strong peaks indicate that the sample is well-ordered. The peaks correspond well to the characteristic (220), (311), (400), (511) and (440) lattice planes of spinel-phase ZCO, at 2θ=31.2°, 36.8°, 44.7°, 59.3°and 65.1°, respectively. All results indicate that the Zn-Co precursors have been transformed into $ZnCo_2O_4$ completely after calcining.[4, 31, 39] The XRD results also suggest that the replacement of Co^{2+} by Zn^{2+} in Co_3O_4 does not cause any adverse change on the spinel-type structure. From further elemental analysis, EDS data of S1 and S2 are displayed in Fig. s1a and Fig. s1b, respectively, which confirm the existence of Zn, Co, O in S1 (S2) and from which we can deduce approximately a molar ratio of Zn/Co=0.5 from the intensity of elemental peaks or atomic percent. Similarly, the XRD pattern (Fig. 3b) and EDS (Fig. S1c) also confirm the spinel structure and existence of Co, O in S3.

For the same purpose, XPS analysis (Fig. 4) was also applied to identify the surface chemical compositions of S1. To complement the XRD analysis, we show Zn 2p, Co 2p and O 1s XPS spectra in Fig. 4a. As a full wide-scan spectrum of the ZCO microspheres, it indicates the existence of Zn, Co, O elements. As depicted in Fig. 4b, two peaks of binding energy values at 1022.6 and 1045.6 eV are evident, which indicate the Zn(II) oxidation state of ZCO.[37, 40] Fig. 4c shows the Co 2p

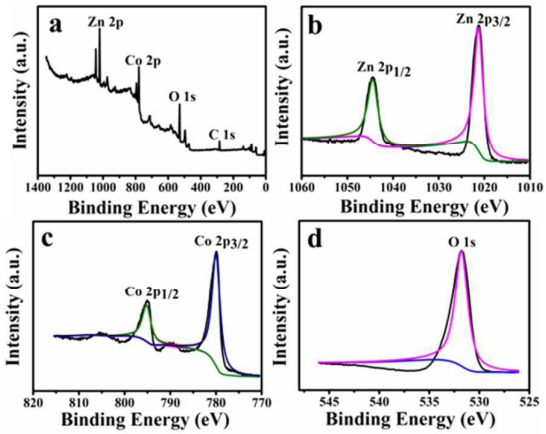

Fig. 4 XPS spectra of as-obtained porous $ZnCo_2O_4$ microspheres: (a) survey, (b) Zn 2p spectrum, (c) Co 2p spectrum and (d) O1s spectrum.

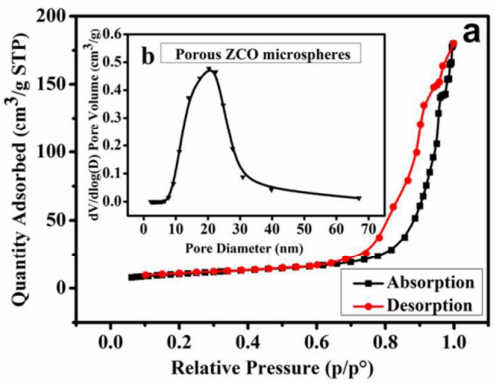

Fig. 5 (a) N_2 adsorption-desorption isotherm of S1, (b) BJH pore-size distribution plot (inset)

spectrum, from which two strong peaks at ca. 794.5 eV for Co $2p_{1/2}$ and 779.8 eV for Co $2p_{3/2}$ are found; these confirm the Co (III) oxidation state of ZCO.[32, 37, 41] The O1s peak (Fig. 4d) at 532.0eV matches the oxygen species in ZCO.[32] Thus, we are able to deduce that the obtained product is $ZnCo_2O_4$ compound with normal spinel structure, combined the all data above.

To verify the porous structure further, N_2 adsorption-desorption isothermal technique (Fig.5) was applied to evaluate the surface structural data of the as-obtained products. The N_2-BET surface area of S1 is calculated as $77.3 m^2 \cdot g^{-1}$, which supplies an adequate surface for gas sensing reactions. The isotherm profile can be classified as type-IV with a hysteresis loop, which indicates the existence of a mesoporous structure in the nano/microstructures. The pore-size distribution (Fig. 5b, the inset) was determined by the BJH method from the desorption branch of the isotherm. The pore diameter of the product was ca.15~40nm (mainly 25nm), which favours mass transportation. The BET data of other samples (S2, S3) are shown in Fig. s2 and are summarized in Table s1. By comparison, S1 has the largest surface area (S1>S3>S2>S4), favourable mesoporous structure, and rough and loose surface, which inevitably result in a sharp leap in gas sensing performance.

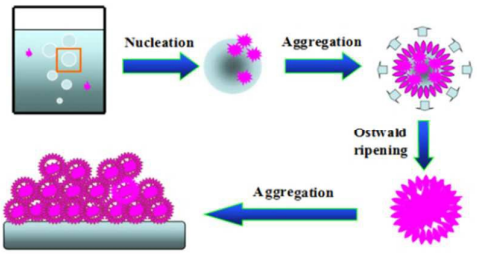

Scheme 1 Schematic illustration of the formation to $ZnCo_2O_4$ microspheres.

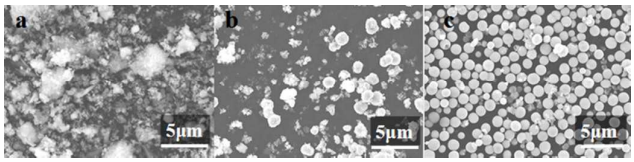

Fig. 6 SEM images of S1 at various reaction times: (a) 1 h, (b) 4 h, and (c) 8 h.

3.3 Formation mechanism

To investigate the formation process of the ZCO porous nano/microsphere, the morphology and structure of the as-prepared S1 at various reaction times are described (schematically in Scheme 1), which is confirmed by SEM images (Fig.6). The time-dependent experiments generally illustrate that the formation of ZCO porous nano/ microsphere is a step-by-step process. During synthesis, Zn^{2+} and Co^{2+} cations are first covered by Eg and Et molecules forming clusters under stirring. Then urea starts to decompose and brings about an alkaline environment and bubbles (soft template). Coupling with Co^{2+} oxidized to Co^{3+} by dissolved oxygen, the cationic clusters hydrolyse under the alkaline environment forming numerous nanoparticles. Afterwards, these nanoparticles tend to aggregate randomly and continue to grow and self-assemble (Ostwald ripening, van der Waals forces, crystal-face attraction etc.) into well-ordered hierarchical microspheres, driven by the so called minimization of surface energy. [37] Next, the microspheres settle down under the action of gravity. The final products are obtained after the two-step calcination treatment. The rough reaction process is illustrated by the following formulas:

$$CO(NH_2)_2 + 3H_2O \rightarrow 2NH_4^+ + 2OH^- + CO_2$$

$$Zn^{2+} + 4Co^{2+} + 4H_2O + 2CO(NH_2)_2 + 3O_2 \rightarrow 2ZnCo_2O_4 + 2CO_2$$

3.3 The gas sensing properties

To demonstrate the potential application of S1 in gas sensing, the four sensors based on various materials stated above are all fabricated to evaluate their gas sensing performance. As acknowledged, the working temperature is a key parameter determining the quality of the gas sensor. Parallel experiments were carried out to determine the optimum operating temperature for soaking in 100ppm ethanol vapour, ranging from 125°C to 350°C. As displayed, we summarize the response of the tested sensors in Fig. 7a. The responses of the tested sensors vary with the operating temperature markedly.

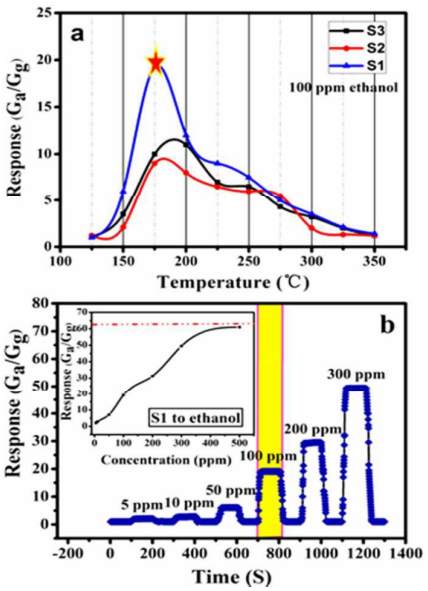

Fig. 7 (a) Response of three samples at different operating temperatures to 100 ppm ethanol, (b) Dynamic sensing response of S1 to 100 ppm ethanol at 175℃ (inset the relationship of response vs. ethanol concentration).

We observe that the responses all increase with the initial operating temperature and reach a maximum value at about 175°C (S1). After achieving the maximum, a distinct decline is observed confirming the existence of an optimal temperature, which is finally taken as 175°C. And Fig.s4b and s4c display the gas sensing performance of S4 (ZCO nanoparticles).[43,44] By contrast, the response of porous ZCO nano/microspheres achieves a peak value of 19.3 based on repeated trials; this is almost twice higher than that of S3 and also higher compared with S2 at the same working temperature. All data indicate that the response of S1 is the highest among our samples, mainly due to the unique loose and porous structure and larger available surface area, which bring more reaction active sites resulting in the promotion of response. Indeed, different GSMs may have different optimal working temperatures to the same tested gas. For pure Co_3O_4 (S3), the maximum value of response obtained is ca.10 at 200°C, which displays comparable properties to reported data.[42]

To highlight the monotonicity of response to concentration further, we summarize the dynamic responses at 175°C in Fig. 7b. Clearly, the sensor based S1 displays an excellent response to ethanol vapour. When the sensor is exposed to air, the response returns nearly to the baseline level. While exposed to ethanol vapour, the response value achieves a maximum and maintains a plateau, which can be explained by the saturation of reaction sites changing little and not causing effective conductivity variation. The nearly square shape observed means that the sensor based on S1 has a rapid response toward tested gas. And from the inset, the response increases with concentration which indicates a stronger monotonous responsiveness. Besides, it is noteworthy that the tendency (inset) of the concentration response approaches near-line at the lower concentration, ranging from 5 to 300 ppm.

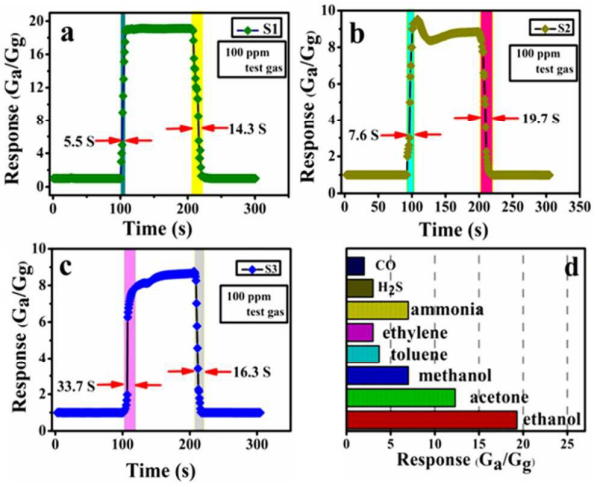

Fig. 8 (a-c) Response/recovery times of three samples (S1, S2, and S3, respectively). (d) Response of sensor based on S1 to 100 ppm various gases at an operating temperature of 175℃.

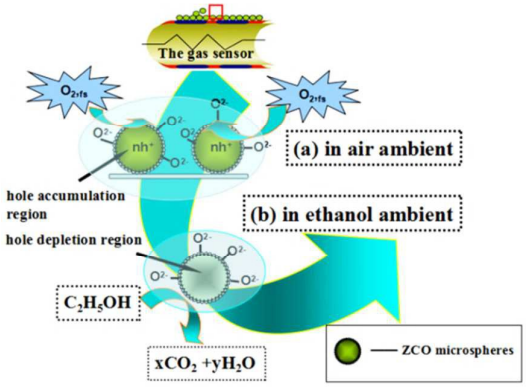

Fig. 9 Schematic diagram of ethanol sensing mechanism of porous $ZnCo_2O_4$ microspheres-based sensor.

The response and recovery times also play a vital part for the practical detection of detrimental gases. Fig. 8 (a-c) shows the response and recovery times of three sensors to 100 ppm tested gases (ethanol). And to make the comparisons more direct, we summarize these in Table s1, The response times are 5.5, 7.6 and 33.7s respectively, while the corresponding recovery times are 14.3, 19.7 and 16.4s respectively. As for S1, the faster response (recovery) time results from the special microsphere structure and the loose, porous surface which favours gas diffusion and mass transport.

The selectivity is also a crucial parameter for the gas sensor. A bar graph (Fig. 8d) of the sensor based on as-obtained ZCO toward a series of gases is displayed, such as methanol, ethanol, acetone and toluene. All gases at a concentration of 100ppm were tested under an optimal temperature (175°C). As shown, the sensors possess excellent selectivity to ethanol in comparison to any other gas at the same concentration (100ppm). The requirement for a reliable and stable gas sensing property is imperative. The cyclic response curves of three sensors were shown in Fig. s3, which displayed a more stable and repeatable performance.

3.4 The gas sensing mechanism

While the sensing mechanism of $ZnCo_2O_4$ has rarely been reported in other works, $ZnCo_2O_4$ is a typical p-type semiconductor oxide and its sensing mechanism can also be explained through the changes in resistance (or conductivity) of the sensor caused by the gas sensing reaction on the surface of the oxides.[20, 30, 42] In combination with all the characterization and test data, we present a sensing process as follows, which also explains the relevance of optimal temperature. Initially, when the surface of p-typed ZCO microspheres is exposed in air, the oxygen (called free state O_2 or $O_{2,fs}$) diffuses to the surface of GSMs, triggering an adsorption reaction to form an adsorbed state O_2 ($O_{2,as}$) at the beginning. Secondly, the $O_{2,\,as}$ captures an electron in the conductive band (CB) of ZCO and changes to an ionic state ($O_{2,\,IS}^-$), producing an h^+. The $O_{2,\,IS}^-$ undergoes a series of electron transfer reactions further forming the final ionic state ($O_{2,\,FIS}^{2-}$), which results in an increase in the accumulation of holes that form regions; these show variation in conductivity.[42] At the third step, when the ZCO surface encounters ethanol (Tg), a crucial reaction occurs between O^{2-}, FIS and the target gas (Tg), consuming some of the holes to form hole depleted regions and again causing variation in conductivity. The resultant from the third step will desorb in air, and the process is repeated. Similarly, for n-type oxide semiconductors, the adsorption of oxygen with negative charge can lead to the formation of an electron-depletion layer (EDL) near the surface; for p-type oxide semiconductors substitution by a hole-accumulation layer (HAL) occurs.[42] HALs can develop on the surface of each of the ZCO particles. As for the hierarchical microspheres, HAL is formed on the entire interior and exterior surface, which decreases sensor resistance after the chemisorption process reaches equilibrium. When the ethanol gas reacts with the oxygen ions absorbed onto the surface, the trapped free electrons are released, which also result in the variation of resistance. Fig. 9 describes the whole sensing process; the reaction is displayed as below: [18]

$$O_{2,\,fs}\,(gas) \rightarrow O_{2,\,as}\,(ads)$$

$$O_{2,\,as}\,(ads) \rightarrow O_{2,\,IS}^-(ads) + h^+$$

$$O_{2,\,IS}^-(ads) \rightarrow 2O^{2-}{}_{FIS}\,(ads) + 3h^+$$

$$C_2H_5OH + 6O^{2-} + 12h^+ \rightarrow 2CO_2 + 3H_2O$$

From the analysis above, we can observe straightaway many factors that can influence the response of the sensors to a certain target gas, such as adsorption capacity toward a certain gas, the decomposition rate of the absorbed molecule at the surface, the concentration of charge carriers in the material, temperature, and the catalytic activity. Herein, our hierarchical 3-D microsphere structures possess loose and porous surfaces, which bring about a large surface area and mass transported channels. These inevitably promote gas absorption and desorption, resulting in an excellent gas sensing performance.

4. Conclusions

In summary, we have reported on a self-assembly method to prepare hierarchical porous ZCO nano/ microspheres by a facile one-step solvothermal process and subsequent annealing treatment. The formation mechanisms of the hierarchical porous ZCO nano/microspheres, constructed by using many nanoparticles, are explained by Ostwald ripening and Kirkendall effect. More importantly, when ZCO porous nano/microspheres were utilized as the sensing material in gas sensors, the almost rectangle response shape obtained to 100 ppm ethanol indicated excellent gas response behaviour. Furthermore, by comparison, great improvements in gas sensing trials occur at ZCO material. The reasons for the enhanced gas sensing properties could be ascribed to high porosity and favourable permeability. ZCO materials also exhibited comparable gas sensing performance and chemical stability to Co_3O_4, suggesting that ZCO could be a more environmental friendly and worthwhile replacement for Co_3O_4. And we anticipate that our researchers can offer a greater inspiration for improving sensing performance of metal oxide semiconductors and the gas sensing properties of ZCO can further improve.

Acknowledgements

We acknowledge the financial supports of the National Natural Science Foundation of China (51402065), Heilongjiang Province Natural Science Funds for Distinguished Young Scholar (JC201404), Special Innovation Talents of Harbin Science and Technology for Distinguished Young Scholar (2014RFYXJ005), Fundamental Research Funds of the Central University (HEUCFZ), Program of International S&T Cooperation special project (2013DFR50060), Special Innovation Talents of Harbin Science and Technology (2013RFQXJ145), and the National Natural Science Foundation of China (61473095).

Notes and references

1 Y. Li and J. Shi, *Adv. mater.*, 2014, **26**, 3176-3205.
2 H.-J. Kim and J.-H. Lee, *Sens. Actuators B: Chemical*, 2014, **192**, 607-627.
3 V. Etacheri, R. Marom, R. Elazari, G. Salitra and D. Aurbach, *Energy & Environmental Science*, 2011, **4**, 3243.
4 S. Wang, Z. Ding and X. Wang, *Chem. commun.*, 2015, **51**, 1517-1519.
5 J.-H. Lee, *Sens. Actuators B: Chemical*, 2009, **140**, 319-336.
6 H. Z. Zhenyu Li, Wei Zheng, Wei Wang, Huimin Huang, and Ce Wang, Alan G. MacDiarmid, and Yen Wei, *J. Am. Chem. Soc,* 2008.
7 J. Li, X. Liu, J. Cui and J. Sun, *ACS appl. Mater. interfaces*, 2015, **7**, 10108-10114.
8 G. Yang, P. Hu, Y. Cao, F. Yuan and R. Xu, *Nanoscale research letters*, 2010, **5**, 1437-1441.
9 G. Duan, F. Lv, W. Cai, Y. Luo, Y. Li and G. Liu, *Langmuir : the ACS journal of surfaces and colloids*, 2010, **26**, 6295-6302.
10 Y. J. Hong, M. Y. Son and Y. C. Kang, *Adv. materials*, 2013, **25**, 2279-2283, 2250.
11 J. Zhang, J. Guo, H. Xu and B. Cao, *ACS applied materials. interfaces*, 2013, **5**, 7893-7898.
12 J. Bai and B. Zhou, *Chemical reviews*, 2014, **114**, 10131-10176.
13 E. Şennik, S. Kerli, Ü. Alver and Z. Z. Öztürk, *Sens. Actuators B: Chemical*, 2015, **216**, 49-56.
14 P. Sun, X. Zhou, C. Wang, K. Shimanoe, G. Lu and N. Yamazoe, *J. Mater. Chem. A*, 2014, **2**, 1302-1308.
15 L. Wang, J. Deng, T. Fei and T. Zhang, *Sens. Actuators B: Chemical*, 2012, **164**, 90-95.
16 E. X. Chen, H. R. Fu, R. Lin, Y. X. Tan and J. Zhang, *ACS appl. Mater. interfaces*, 2014, **6**, 22871-22875.
17 S. Park, S. Kim, G. J. Sun and C. Lee, *ACS appl. Mater. interfaces*, 2015, **7**, 8138-8146.
18 Y. Bing, Y. Zeng, C. Liu, L. Qiao and W. Zheng, *Nanoscale*, 2015, **7**, 3276-3284.
19 Y. Q. Liang, Z. D. Cui, S. L. Zhu, Z. Y. Li, X. J. Yang, Y. J. Chen and J. M. Ma, *Nanoscale*, 2013, **5**, 10916-10926.
20 Y. Lu, W. Zhan, Y. He, Y. Wang, X. Kong, Q. Kuang, Z. Xie and L. Zheng, *ACS appl. Mater. interfaces*, 2014, **6**, 4186-4195.
21 N. Kavasoğlu, A. S. Kavasoğlu and M. Bayhan, *Sens. Actuators A: Physical*, 2006, **126**, 355-361.
22 W. Wang, H. Chai, X. Wang, X. Hu and X. Li, *Applied Surface Science*, 2015, **341**, 43-47.
23 D. Bekermann, A. Gasparotto, D. Barreca, C. Maccato, E. Comini, C. Sada, G. Sberveglieri, A. Devi and R. A. Fischer, *ACS appl. Mater. interfaces*, 2012, **4**, 928-934.
24 W.S. Kim, Y. Hwa, H.C. Kim, J.H. Choi, H. J. Sohn and S.H. Hong, *Nano Research*, 2014, **7**, 1128-1136.
25 X. W. Lou, D. Deng, J. Y. Lee and L. A. Archer, *J. Mater. Chem.*, 2008, **18**, 4397.
26 S. Shafiu, H. Kavas and A. Baykal, *Journal of Super conductivity and Novel Magnetism*, 2014, **27**, 1751-1755.
27 Y. Wang, Y. Lei, J. Li, L. Gu, H. Yuan and D. Xiao, *ACS appl. Mater. interfaces*, 2014, **6**, 6739-6747.
28 X. Zhang, Y. Zhao and C. Xu, *Nanoscale*, 2014, **6**, 3638-3646.
29 X. Wang, W. Tian, T. Zhai, C. Zhi, Y. Bando and D. Golberg, *J. Mater. Chem.*, 2012, **22**, 23310.
30 F. Qu, J. Liu, Y. Wang, S. Wen, Y. Chen, X. Li and S. Ruan, *Sens. Actuators B: Chemical*, 2014, **199**, 346-353.
31 X. Zhou, W. Feng, C. Wang, X. Hu, X. Li, P. Sun, K. Shimanoe, N. Yamazoe and G. Lu, *J. Mater. Chem. A*, 2014, **2**, 17683-17690.
32 S. Vijayanand, P. A. Joy, H. S. Potdar, D. Patil and P. Patil, *Sens. Actuators B: Chemical*, 2011, **152**, 121-129.
33 G. Zhang, L. Yu, H. B. Wu, H. E. Hoster and X. W. Lou, *Adv. Mater.*, 2012, **24**, 4609-4613.
34 M. Fleischer, *Measurement Science and Technology*, 2008, **19**, 042001.
35 X. Niu, W. Du and W. Du, *Sens. Actuators B: Chemical*, 2004, **99**, 405-409.
36 X. Wang, W. Liu, J. Liu, F. Wang, J. Kong, S. Qiu, C. He and L. Luan, *ACS appl. Mater. interfaces*, 2012, **4**, 817-825.
37 L. Hu, B. Qu, C. Li, Y. Chen, L. Mei, D. Lei, L. Chen, Q. Li and T. Wang, *J. Mater. Chem. A*, 2013, **1**, 5596.
38 K. B. Gawande, S. B. Gawande, S. R. Thakare, V. R. Mate, S. R. Kadam, B. B. Kale and M. V. Kulkarni, *RSC Adv.*, 2015, **5**, 40429-40436.
39 Y. Sharma, N. Sharma, G. V. S. Rao and B. V. R. Chowdari, *Adv. Funct. Mater.*, 2007, **17**, 2855-2861.
40 B. P. a. W. U. I. Grohmann, *Surface and Interface Analysis*, 1992.
41 T. W. Kim, M. A. Woo, M. Regis and K.-S. Choi, *The Journal of Physical Chemistry Letters*, 2014, **5**, 2370-2374.
42 J. Deng, R. Zhang, L. Wang, Z. Lou and T. Zhang, *Sens. Actuators B: Chemical*, 2015, **209**, 449-455.
43 R. D. P. a. S. R. B. Sachin. V. Bangale, *J. Chem. Pharm. Res.*, 2011, **3**, 527-535
44 C. R. Mariappan, R. Kumar and G. Vijaya Prakash, *RSC Adv.*, 2015, **5**, 26843-26849.